

One-sided Competition of Charge-Density-Wave order and Superconductivity in 2H-NbSe₂

Owen Moulding,¹ Israel Osmond,¹ Felix Flicker,² Takaki Muramatsu,¹ and Sven Friedemann^{1, *}

¹*HH Wills Laboratory, University of Bristol, Bristol, BS8 1TL, UK*

²*Rudolf Peierls Centre for Theoretical Physics, University of Oxford, Department of Physics, Clarendon Laboratory, Parks Road, Oxford, OX1 3PU, United Kingdom*

(Dated: Tuesday 24th May, 2022)

The interplay of incompatible ground states is a key concept in physics and central to many materials classes from monolayer graphene and transition metal dichalcogenides to cuprate high-temperature superconductors. Tuning the balance between these ground states reveals competition, coexistence, and cooperation - sometimes even within the same system. Here, we present comprehensive high-pressure Hall effect and magnetic susceptibility measurements of the charge-density-wave (CDW) and superconducting state in 2H-NbSe₂. We show that superconductivity is enhanced upon suppressing CDW order at high pressures whilst CDW order is insensitive to a suppression of superconductivity in high magnetic fields. With a realistic model calculation we show that the suppression of the CDW state at high pressures is described by the stiffening of the underlying bare phonon modes, whilst the suppression of the superconducting state at low pressures is due to the loss of density of states inside the CDW phase. We conclude that the competition between the two states is one-sided in 2H-NbSe₂. Our work clarifies the interplay of superconductivity and CDW order in prototypical 2H-NbSe₂ and highlights routes to optimise superconductivity in materials with competing order.

The interplay of competing orders is of fundamental and practical interest [1–4]. Controlled switching between phases promises new applications in data storage and sensing [1]. On a fundamental level, understanding the interplay between ground states provides important insight into the mechanism underlying each ground state and can reveal new phenomena at the border of ordered phases [3, 5]. For instance, a large body of work focuses on the interplay of superconductivity and charge order in cuprate high-temperature superconductors [4, 6].

With both superconductivity and charge-density-wave (CDW) order ensuing from the opening of a gap on (parts of) the Fermi surface, a mutual competition between the two states was originally expected [7–9]. As an alternative, superconductivity in a dome around quantum critical points was suggested to be promoted by quantum fluctuations of the ordered state with prominent examples in heavy-fermion antiferromagnets [10], CDW systems [11], and the CDW and pseudogap order in cuprate superconductors [12]. In addition to competition and promotion, superconductivity and charge order can coexist for instance by opening a gap on different parts of the Fermi surface. 2H-NbSe₂ is a prototypical material hosting both CDW order and superconductivity.

The interplay of CDW order and superconductivity in 2H-NbSe₂ remains disputed [13, 14]. CDW order sets in at $T_{\text{CDW}} \sim 33$ K while superconductivity is present below $T_c = 7.1$ K at ambient pressure [15–18]. Superconductivity opens gaps of different size on most of the Fermi surface while the CDW opens a gap on small parts of the zone-corner niobium-derived Fermi surface sheets only [13, 14, 16, 19–22]. The separation of the CDW and superconducting gaps in k -space was interpreted as a

hallmark for coexistence of the two ordered states but further studies suggested that superconductivity is boosted by CDW order [13], some studies suggested a promotion of superconductivity by the soft modes present at the quantum critical point of the CDW order [23, 24], and some studies suggested a mutual competition for density of states between the CDW and superconductivity [14, 25, 26]. Here, we use comprehensive high-pressure and magnetic field tuning of the CDW and superconducting states to reveal a partial but one-sided competition of the CDW with the superconductivity. We find that the suppression of CDW order with pressure is correlated with a rise in T_c , but a suppression of the superconductivity by magnetic field does not yield a rise in T_{CDW} .

Our high-pressure Hall effect measurements show the suppression of T_{CDW} under pressure in Fig. 1. At high temperatures, the Hall coefficient, R_{H} , is weakly temperature dependent and does not change with pressure. At T_{CDW} , $R_{\text{H}}(T)$ shows a large drop and a sign change naturally associated with the Fermi surface reconstruction due to the CDW [27, 28]. The contribution to the Hall coefficient from the CDW, $\Delta R_{\text{H}}(T, P) = R_{\text{H}}(T, P) - R_{\text{H}}(T, 5.5 \text{ GPa})$, is calculated by subtracting the non-CDW form well above the critical pressure. In the derivative $d\Delta R_{\text{H}}/dT$, the CDW transition manifests as a pronounced peak as shown in Fig. 1(b). $T_{\text{CDW}}(P)$ associated with the maximum in $d\Delta R_{\text{H}}/dT$ shifts to lower temperature as pressure is increased in good agreement with $T_{\text{CDW}}(P)$ extracted from resistivity measurements as well as with previous results of T_{CDW} as highlighted in Fig. 2 and in section SI of the supplemental information. The benefit of analysing the Hall coefficient is that the strong signature can be traced to higher pressures where

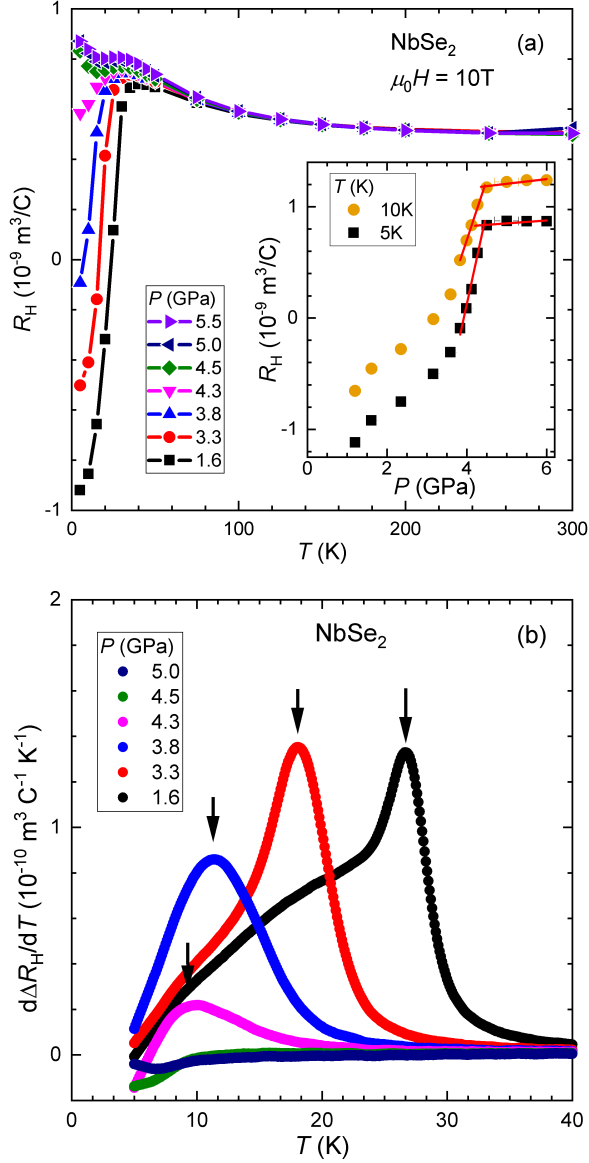


FIG. 1. **Suppression of the CDW transition in 2H-NbSe₂ under pressure.** (a) The temperature dependence of the Hall coefficient. Inset shows the pressure dependence $R_H(P)$ measured at $\mu_0 H = 10$ T at selected temperatures. Straight lines highlight linear fits to the data. (b) Derivative of the Hall coefficient ($d\Delta R_H/dT$) was calculated after subtracting the high-pressure background, i.e. $\Delta R_H(T, P) = R_H(P, T) - R_H(T, P = 5.5 \text{ GPa})$. Arrows indicate T_{CDW} extracted as the maximum.

the signature in resistivity is lost (cf. Ref [29]). We observe the CDW transition in $\Delta R_H(T)$ up to a pressure of 4.3 GPa.

The suppression of T_{CDW} is confirmed by the isothermal pressure dependency of the Hall coefficient $R_H(P)$ shown in the inset of Fig. 1(a). $R_H(P)$ exhibits a pronounced kink associated with the critical pressure of the CDW phase, $P_{CDW}(T)$ (cf. intersecting linear fits in the

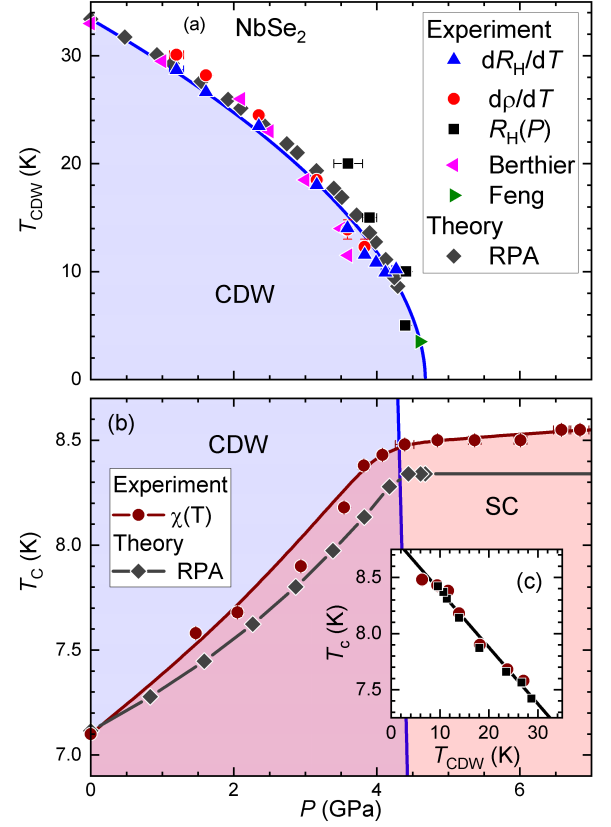


FIG. 2. **High-pressure phase diagram of 2H-NbSe₂.** (a) Experimental values of $T_{CDW}(P)$ are determined as the peak in $d\Delta R_H/dT$ as shown in Fig. 1, as the minimum in $d\rho/dT$ as shown in SI, and the kink in $R_H(P)$ as shown the inset of Fig.1(a). Theoretical values of $T_{CDW}(P)$ are calculated as described in methods section S V and section S VI of the Supplementary Material. Data from Refs. [23, 29] are included. The solid line marks a power-law fit to our experimental datasets of $T_{CDW}(P)$. (b) Experimental results for $T_c(P)$ are extracted from magnetisation measurements (Fig. 3). A detailed comparison of $T_c(P)$ using different pressure media is given in S I. Theoretical values of $T_c(P)$ are calculated as described in S VI. The boundary of the CDW phase is reproduced from (a). Inset (c) shows the relation of the superconductivity and CDW transition temperatures. The solid line is a linear fit.

inset of Fig. 1(a)). The position of $P_{CDW}(T)$ is included as black squares in the phase diagram in Fig. 2. $P_{CDW}(T)$ becomes virtually independent of temperature for $T \leq 10$ K, i.e. the kink in $R_H(P)$ is found at virtually the same pressure $P_{CDW}(T) = 4.4$ GPa for 5 K and 10 K. In section SII of the supplementary information we show that this result is also true if the Hall effect is probed in smaller magnetic fields. $R_H(P)$ indicates a sharp decrease of $T_{CDW}(P)$ which could be interpreted as signature of a first order transition at high pressures. This is further supported by the fact, that the amplitude of the CDW anomaly in $\Delta R_H(T)$ diminishes at 4.3(1) GPa as shown in section S II of the supplemental information.

However, no signs of first order have been observed in x-ray diffraction and models of the CDW including our model below exclude a change from second to first order at high pressures [23, 30].

Our results are consistent with previous X-ray diffraction measurements within experimental uncertainties [23, 30]. The critical pressure from the XRD studies is included as a green triangle in Fig. 2(a). Our comprehensive Hall effect measurements provide for the first time a single dataset tracing $T_{\text{CDW}}(P)$ to the critical pressure. We fit the phase boundary extracted from our $R_{\text{H}}(T)$ and $R_{\text{H}}(P)$ datasets with a power-law yielding an exponent 0.5(1) and an extrapolated critical pressure $P_{\text{CDW}} = 4.7(1)$ GPa (cf. solid line in Fig. 2(a)).

Superconductivity is boosted under pressure in clear anticorrelation to the CDW. $T_{\text{c}}(P)$ is traced as the onset of the diamagnetic signal in magnetic susceptibility measurements, χ , as presented in Fig. 3. The sharp onset gives $T_{\text{c}} = 7.1$ K at ambient pressure in good agreement with our resistivity measurements (cf. S I of the supplementary information) and other published work [17, 18]. With increasing pressure, $T_{\text{c}}(P)$ shifts to higher temperature whilst the transition remains very sharp. Above 4.4 GPa, $T_{\text{c}}(P)$ saturates at 8.5 K. The measurements presented in Fig. 3 used argon as a pressure transmitting medium (PTM) which remains hydrostatic up to 11 GPa [31]. We find very good agreement with $T_{\text{c}}(P)$ extracted from our resistivity measurements up to 5.5 GPa – the limiting pressure for hydrostaticity of the PTM glycerol used for the electrical transport measurements. The comparison of different PTM and literature data in section S I show that the measurements with argon and glycerol (up to 5.5 GPa) reveal the intrinsic behaviour of superconductivity in 2H-NbSe₂.

The evolution of $T_{\text{c}}(P)$ is shown in Fig. 2(b) together with the phase boundary of the CDW order established from our transport measurements. $T_{\text{c}}(P)$ is virtually constant for $P \geq 4.4$ GPa, i.e. outside the CDW phase. At the same time, T_{c} is reduced by up to 1.4 K inside the CDW phase in clear anticorrelation with $T_{\text{CDW}}(P)$ as highlighted in Fig. 2(c). We do not observe a maximum in T_{c} around the critical pressure of the CDW phase, and thus rule out a boost to superconductivity from the CDW critical fluctuations.

A detailed model using a structured electron-phonon coupling shows that the suppression of the CDW under pressure is driven by the stiffening of the underlying bare phonon. In Fig. 2, the experimental transition temperatures are compared to the detailed model of the charge order and Fermi surface developed earlier by one of us as outlined in sections S V and S VI of the supplementary material [32–34]. In our RPA calculations, the overall magnitude of the electron-phonon coupling \mathbf{g} is constrained to reproduce $T_{\text{CDW}}(P = 0) = 33.4$ K (cf. S III of the supplementary information) and we keep \mathbf{g} fixed for all pressures. To describe $T_{\text{CDW}}(P)$, we assume a linear

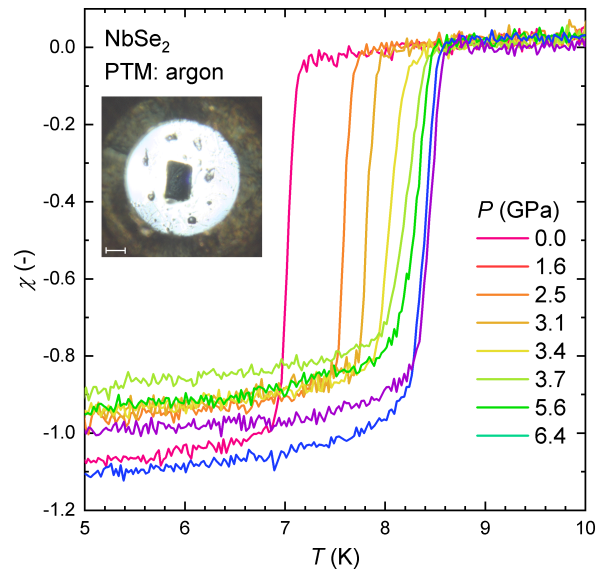


FIG. 3. **Enhanced superconductivity in 2H-NbSe₂ under pressure.** The volume susceptibility χ measured on warming the sample in a magnetic field $\mu_0 H = 0.5$ mT after zero-field cooling. The transition into the superconducting state inferred from the diamagnetic signal shifts to higher temperatures as the pressure is increased. Inset shows a picture of the sample and ruby chips inside the pressure cell. Argon was used as a pressure medium.

stiffening of the longitudinal acoustic phonons underlying the CDW formation consistent with high-pressure inelastic x-ray studies [35] as detailed in section S V of the supplementary information. From the good match with the experimental phase boundary, we conclude that the suppression of the CDW is indeed driven by the increase of the bare phonon frequency whilst the electron-phonon constant remains unchanged.

A partial competition for density of states (DOS) is the main driver for the evolution of $T_{\text{c}}(P)$. We use the experimentally determined phase boundary (solid line in Fig. 2(a)) to scale the evolution of the CDW phase to our pressure data as detailed in section S VI of the supplementary information. Inside the CDW phase, the DOS available for superconductivity is reduced due to the gapping of the inner K-pockets of the Fermi surface as illustrated in Fig. 4 leading to a reduction of T_{c} . As the CDW gap becomes smaller, the DOS available for superconductivity becomes larger which in turn accounts for almost the entire increase of T_{c} and naturally explains why T_{c} saturates above P_{CDW} as can be seen in Fig. 2(b). Thus, we conclude that it is a partial competition for DOS which suppresses T_{c} inside the CDW phase.

A suppression of the CDW order inside the superconducting phase is not observed. At zero pressure, no reduction in the X-ray intensity of the CDW reflection is observed at T_{c} [15, 36]. At pressures up to 4.4 GPa, the

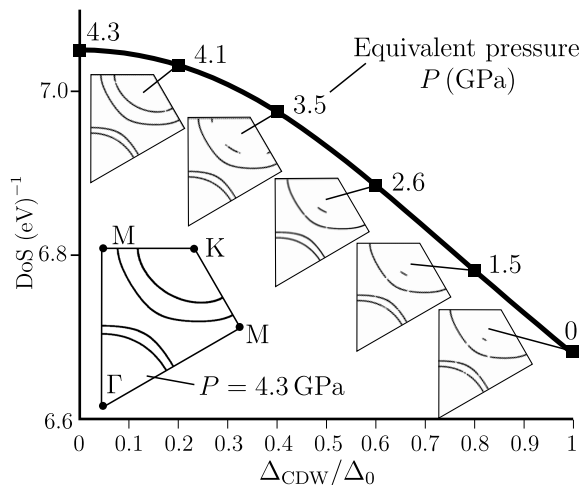


FIG. 4. Reduction of DOS as a function of CDW gap magnitude for the two Nb-derived bands at E_F . Insets show the Fermi surface in a wedge of the Brillouin zone for specific values of Δ_{CDW} and equivalent pressure. The plotted points were identified as the points at which the RPA spectral function is within 15% of its maximum value.

CDW order is detected with X-ray diffraction inside the SC state [23, 30]. At pressures above 4.4 GPa, the CDW is absent in high fields, i.e. outside the superconducting phase and thus cannot be suppressed below the critical field of the superconducting phase. This finding is consistent with the above modelling showing that the suppression of the CDW is driven by the stiffening of the bare phonon whilst the suppression of the superconductivity is driven by the partial competition for DOS.

Our results lead to several profound conclusions about the interplay of CDW order and superconductivity in 2H-NbSe₂. (i) The CDW order is reducing the electronic density of states available for superconductivity leading to a reduction of T_c . (ii) Superconductivity is not reducing T_{CDW} . Hence, (iii) the competition between CDW order and superconductivity is not mutual but rather one-sided with only superconductivity suppressed by CDW order but not the other way around. (iv) No signature of a boost to superconductivity from CDW fluctuations has been observed.

In summary, we conclude that the competition between the CDW and superconducting states is one-sided in 2H-NbSe₂, clarifying the prototypical nature of 2H-NbSe₂. Crucially, 2H-NbSe₂ shows markedly different behaviour compared to cuprate superconductors where T_c increases under pressure despite no change to T_{CDW} up to 3 GPa [6]. The interplay of coexisting states is a central focus of current physics, of interest both in its own right as an intriguing theoretical puzzle, but also owing to potentially wide-ranging applications such as clarifying the origins of high-temperature superconductors. The results presented here reveal the precise form of the interplay between the low-temperature states in a prototypical test-

case, helping pave the way for understanding the idea in its broader context.

METHODS

Samples

2H-NbSe₂ samples were grown by J. A. Wilson [17] using the vapour transport method and showed a high residual resistivity ratio, $\rho(T = 300 \text{ K})/\rho(T = 9 \text{ K}) = 64$, confirming the good crystal quality. Samples were cut with a scalpel. Lateral sample dimensions have been obtained with an optical microscope at ambient pressure (see inset in Fig. 3), sample thickness, t , was estimated from the sample mass and the lateral dimensions using the known density of 2H-NbSe₂. The associated uncertainty of 10% results in a systematic relative uncertainty of the Hall coefficient of the same amount. The magnetic field was applied along the crystallographic c direction.

High-Pressure Measurements

High-pressure measurements used moissanite anvils cells with a culet size of 800 μm for both the electrical and magnetic measurements. Both types of measurement used metallic gaskets which were prepared by indenting 450 μm thick BeCu to approximately 60 μm followed by drilling a 450 μm hole.

Pressure was determined at room temperature by ruby fluorescence, with multiple ruby flakes placed within the sample chamber as a manometer. The uncertainty of the pressure is taken as the standard deviation between pressure estimates from rubies across the sample chamber, both before and after a measurement. A comparison with the pressure obtained from ruby at room temperature and the superconducting transition of a piece of lead revealed good agreement to within 0.2 GPa for the pressure cells used for magnetisation measurements.

Electrical Transport Measurements

For the electrical measurements, six bilayer electrodes were deposited on one anvil in a three-step process without breaking vacuum. Firstly, the anvil was cleaned using an RF argon plasma etch, followed by sputtering 20 nm of nichrome, and finally evaporation of 150 nm gold. To ensure no electrical short between electrodes, any nichrome overspray was removed using TFN etchant.

Gold contacts were evaporated on top of the sample. Epo-Tek H20E silver paint was used to connect the samples to the electrodes on the anvil. A four-probe AC method was used to measure the resistance with a current $I = 1 \text{ mA}$. The six electrodes were used to measure

V_l , the longitudinal and V_t , the transverse voltages, respectively. The Hall coefficient was calculated from the antisymmetric part of $V_t(H)$ under reversal of the magnetic field H as

$$R_H = \frac{V_t(H) - V_t(-H)}{2H} \frac{t}{I}.$$

The effect of different pressure media is discussed in S I of the supplementary information.

For the electrical measurements, the gaskets were insulated using a mixture of Stycast epoxy 2850FT and BN powder; the mixture was pressed between the anvils to above the maximum pressure required for the experiments and then cured whilst pressurised. A 400 μm hole through the insulation was drilled for the sample space.

Magnetic Measurements

A Quantum Design Magnetic Property Measurement System (MPMS) was used to measure the DC magnetic moment of the sample inside the pressure cell as detailed in section S IV of the supplementary information. The transition temperature, T_c , has been determined as the temperature where $\chi(T)$ has dropped by 10% of the normalised step, i.e. close to the onset of the transition. This procedure results in uncertainty less than 0.05 K of T_c .

ACKNOWLEDGEMENTS

The authors would like to thank Jasper van Wezel, Jans Henke, Nigel Hussey, Hermann Suderow, and Antony Carrington for valuable discussion. The authors acknowledge supported by the EPSRC under grants EP/R011141/1, EP/L025736/1, EP/N026691/1 as well as the ERC Horizon 2020 programme under grant 715262-HPSuper.

The research data supporting this publication can be accessed through the University of Bristol data repository [37].

AUTHOR CONTRIBUTIONS

OM and SF conducted the electrical transport measurements, IO conducted the magnetic measurements. TM assisted with the high-pressure setups. FF performed the calculations. SF, OM, IO, and FF wrote the manuscript. The project was devised and led by SF.

ADDITIONAL INFORMATION

Data are available at the University of Bristol data repository, data.bris, at <https://doi.org/10.5523/bris.xxxx> [37].

COMPETING INTERESTS

The authors declare that no competing interests are present.

* Sven.Friedemann@bristol.ac.uk

- [1] M. Nakano, K. Shibuya, D. Okuyama, T. Hatano, S. Ono, M. Kawasaki, Y. Iwasa, and Y. Tokura, Collective bulk carrier delocalization driven by electrostatic surface charge accumulation, *Nature* **487**, 459 (2012).
- [2] B. Baek, W. H. Rippard, S. P. Benz, S. E. Russek, and P. D. Dresselhaus, Hybrid superconducting-magnetic memory device using competing order parameters, *Nature Communications* **5**, 3888 (2014).
- [3] S. Friedemann, W. J. Duncan, M. Hirschberger, T. W. Bauer, R. K uchler, A. Neubauer, M. Brando, C. Pfleiderer, and F. M. Grosche, Quantum tricritical points in NbFe_2 , *Nat. Phys.* **14**, 62–67 (2018), [arXiv:1709.05099](https://arxiv.org/abs/1709.05099).
- [4] J. Chang, E. Blackburn, A. T. Holmes, N. B. Christensen, J. Larsen, J. Mesot, R. Liang, D. A. Bonn, W. N. Hardy, A. Watenphul, M. v. Zimmermann, E. M. Forgan, and S. M. Hayden, Direct observation of competition between superconductivity and charge density wave order in $\text{YBa}_2\text{Cu}_3\text{O}_{6.67}$, *Nat. Phys.* **8**, 871 (2012).
- [5] C. Lester, S. Ramos, R. S. Perry, T. P. Croft, R. I. Bewley, T. Guidi, P. Manuel, D. D. Khalyavin, E. M. Forgan, and S. M. Hayden, Field-tunable spin-density-wave phases in $\text{Sr}_3\text{Ru}_2\text{O}_7$, *Nat. Mater.* **14**, 373 (2015).
- [6] C. Putzke, J. Ayres, J. Buhot, S. Licciardello, N. E. Hussey, S. Friedemann, and A. Carrington, Charge order and superconductivity in underdoped $\text{YBa}_2\text{Cu}_3\text{O}_{7-\delta}$ under pressure, *Phys. Rev. Lett.* **120**, 117002 (2018).
- [7] G. Bilbro and W. McMillan, Theoretical model of superconductivity and the martensitic transformation in A15 compounds, *Phys. Rev. B* **14**, 1887 (1976).
- [8] M. Nunez-Regueiro, Extension of Bilbro-McMillan charge density wave-superconductivity coexistence relation to quantum regimes: Application to superconducting domes around quantum critical points, *J. Magn. Magn. Mater.* **376**, 25 (2015).
- [9] G. Grissonnanche, O. Cyr-Choini re, F. Lalibert e, S. Ren e de Cotret, A. Juneau-Fecteau, S. Dufour-Beaus ejour, M.- . Delage, D. LeBoeuf, J. Chang, B. J. Ramshaw, D. A. Bonn, W. N. Hardy, R. Liang, S. Adachi, N. E. Hussey, B. Vignolle, C. Proust, M. L. Sutherland, S. Kr amer, J.-H. Park, D. Graf, N. Doiron-Leyraud, and L. Taillefer, Direct measurement of the upper critical field in cuprate superconductors., *Nat. Commun.* **5**, 3280 (2014).
- [10] N. D. Mathur, F. M. Grosche, S. R. Julian, I. R. Walker, D. M. Freye, R. K. W. Haselwimmer, and G. G. Lonzarich, Magnetically mediated superconductivity in heavy fermion compounds, *Nature* **394**, 39 (1998).
- [11] E. Morosan, H. W. Zandbergen, B. S. Dennis, J. W. G. Bos, Y. Onose, T. Klimczuk, A. P. Ramirez, N. P. Ong, and R. J. Cava, Superconductivity in Cu_xTiSe_2 , *Nat. Phys.* **2**, 544 (2006).

- [12] B. J. Ramshaw, S. E. Sebastian, R. D. McDonald, J. Day, B. S. Tan, Z. Zhu, J. B. Betts, R. Liang, D. A. Bonn, W. N. Hardy, and N. Harrison, Quasiparticle mass enhancement approaching optimal doping in a high- T_c superconductor, *Science* **348**, 317 (2015), [arXiv:1409.3990](https://arxiv.org/abs/1409.3990).
- [13] T. Kiss, T. Yokoya, A. Chainani, S. Shin, T. Hanaguri, M. Nohara, and H. Takagi, Charge-order-maximized momentum-dependent superconductivity, *Nat. Phys.* **3**, 720 (2007).
- [14] S. V. Borisenko, A. A. Kordyuk, V. B. Zabolotnyy, D. S. Inosov, D. Evtushinsky, B. Büchner, A. N. Yaresko, A. Varykhalov, R. Follath, W. Eberhardt, L. Patthey, H. Berger, and B. Buchner, Two Energy Gaps and Fermi-Surface "Arcs" in NbSe₂, *Phys. Rev. Lett.* **102**, 166402 (2009).
- [15] D. E. Moncton, J. D. Axe, and F. J. DiSalvo, Study of Superlattice Formation in 2H-NbSe₂ and 2H-TaSe₂ by Neutron Scattering, *Phys. Rev. Lett.* **34**, 734 (1975).
- [16] T. Yokoya, T. Kiss, A. Chainani, S. Shin, M. Nohara, and H. Takagi, Fermi surface sheet-dependent superconductivity in 2H-NbSe₂, *Science* **294**, 2518 (2001).
- [17] J. A. Wilson and A. Yoffe, The transition metal dichalcogenides discussion and interpretation of the observed optical, electrical and structural properties, *Adv. Phys.* **18**, 193 (1969).
- [18] A. Wieteska, B. Foutty, Z. Guguchia, F. Flicker, B. Mazel, L. Fu, S. Jia, C. Marianetti, J. van Wezel, and A. Pasupathy, Uniaxial Strain Tuning of Superconductivity in 2H-NbSe₂, [arXiv:1903.05253](https://arxiv.org/abs/1903.05253) [cond-mat.supr-con] (2019), <http://arxiv.org/abs/1903.05253v1>.
- [19] D. J. Rahn, S. Hellmann, M. Kalläne, C. Sohrt, T. K. Kim, L. Kipp, and K. Rossnagel, Gaps and kinks in the electronic structure of the superconductor 2H-NbSe₂ from angle-resolved photoemission at 1 K, *Phys. Rev. B* **85**, 224532 (2012).
- [20] T. Valla, A. Fedorov, P. Johnson, P.-A. Glans, C. McGuinness, K. Smith, E. Andrei, and H. Berger, Quasiparticle Spectra, Charge-Density Waves, Superconductivity, and Electron-Phonon Coupling in 2H-NbSe₂, *Phys. Rev. Lett.* **92**, 086401 (2004).
- [21] J. D. Fletcher, A. Carrington, P. Diener, P. Rodière, J. Brison, R. Prozorov, T. Olheiser, and R. Giannetta, Penetration Depth Study of Superconducting Gap Structure of 2H-NbSe₂, *Phys. Rev. Lett.* **98**, 057003 (2007).
- [22] J. A. Galvis, E. Herrera, C. Berthod, S. Vieira, I. Guilmón, and H. Suderow, Tilted vortex cores and superconducting gap anisotropy in 2H-NbSe₂, *Communications Physics* **1**, 30 (2018).
- [23] Y. Feng, J. Wang, R. Jaramillo, J. van Wezel, S. Haravifard, G. Srajer, Y. Liu, Z.-A. Xu, P. B. Littlewood, and T. F. Rosenbaum, Order parameter fluctuations at a buried quantum critical point., *Proc. Natl. Acad. Sci. U. S. A.* **109**, 7224 (2012).
- [24] H. Suderow, V. Tissen, J. Brison, J. Martínez, and S. Vieira, Pressure Induced Effects on the Fermi Surface of Superconducting 2H-NbSe₂, *Phys. Rev. Lett.* **95**, 117006 (2005).
- [25] B. J. Dalrymple and D. E. Prober, Upper critical fields of the superconducting layered compounds Nb_{1-x}Ta_xSe₂, *Journal of Low Temperature Physics* **56**, 545 (1984).
- [26] K. Cho, M. Kończykowski, S. Teknowijoyo, M. A. Tanatar, J. Guss, P. B. Gartin, J. M. Wilde, A. Kreyssig, R. J. McQueeney, A. I. Goldman, V. Mishra, P. J. Hirschfeld, and R. Prozorov, Using controlled disorder to probe the interplay between charge order and superconductivity in nbse2, *Nature Communications* **9**, 2796 (2018).
- [27] K. Yamaya and T. Sambongi, Low-temperature crystal modification and the superconductive transition temperature of NbSe₂, *Solid State Communications* **11**, 903 (1972).
- [28] P. Knowles, B. Yang, T. Muramatsu, O. Moulding, J. Buhot, C. J. Sayers, E. Da Como, and S. Friedemann, Fermi surface reconstruction and electron dynamics at the charge-density-wave transition in tise₂, *Phys. Rev. Lett.* **124**, 167602 (2020), <http://arxiv.org/abs/1911.01945v1>.
- [29] C. Berthier, P. Molinié, and D. Jérôme, Evidence for a connection between charge density waves and the pressure enhancement of superconductivity in 2H-NbSe₂, *Solid State Commun.* **18**, 1393 (1976).
- [30] Y. Feng, J. van Wezel, J. Wang, F. Flicker, D. M. Silivitch, P. B. Littlewood, and T. F. Rosenbaum, Itinerant density wave instabilities at classical and quantum critical points, *Nature Physics* **11**, 865 (2015).
- [31] N. Tateiwa and Y. Haga, Evaluations of pressure-transmitting media for cryogenic experiments with diamond anvil cell., *Rev. Sci. Instrum.* **80**, 123901 (2009).
- [32] F. Flicker and J. van Wezel, Charge order from orbital-dependent coupling evidenced by NbSe₂, *Nature Communications* **6**, 7034 (2015).
- [33] F. Flicker and J. van Wezel, Charge ordering geometries in uniaxially strained NbSe₂, *Phys. Rev. B* **92**, 201103 (2015).
- [34] F. Flicker and J. van Wezel, Charge order in NbSe₂, *Phys. Rev. B* **94**, 235135 (2016).
- [35] M. Leroux, I. Errea, M. Le Tacon, S.-M. Souliou, G. Garbarino, L. Cario, A. Bosak, F. Mauri, M. Calandra, and P. Rodière, Strong anharmonicity induces quantum melting of charge density wave in 2H-NbSe₂ under pressure, *Phys. Rev. B* **92**, 140303 (2015).
- [36] C.-H. Du, W. J. Lin, Y. Su, B. K. Tanner, P. D. Hatton, D. Casa, B. Keimer, J. P. Hill, C. S. Oglesby, and H. Hohl, X-ray scattering studies of 2H-NbSe₂, a superconductor and charge density wave material, under high external magnetic fields, *J. Phys. Condens. Matter* **12**, 5361 (2000).
- [37] O. Moulding, [Doi: 10.5523/bris.xxx](https://doi.org/10.5523/bris.xxx), Data repository for 2H-NbSe₂ article 2020 (2020).

Supplementary Information for “One-sided Competition of Charge-Density-Wave order and Superconductivity in 2H-NbSe₂”

Owen Moulding,¹ Israel Osmond,¹ Felix Flicker,² Takaki Muramatsu,¹ and Sven Friedemann^{1,*}

¹*HH Wills Laboratory, University of Bristol, Bristol, BS8 1TL, UK*

²*Rudolf Peierls Centre for Theoretical Physics, University of Oxford, Department of Physics,
Clarendon Laboratory, Parks Road, Oxford, OX1 3PU, United Kingdom*

(Dated: Friday 5th June, 2020)

INFLUENCE OF PRESSURE MEDIA AND SAMPLE PREPARATION ON SUPERCONDUCTIVITY

We have studied the influence of different pressure media and sample preparation on superconductivity under pressure in 2H-NbSe₂. In Fig. S1(a) we provide a comparison of two different pressure media used in this study: argon and glycerol. Argon was used for the measurements of the magnetic susceptibility presented in Fig. 3 of the main manuscript. Glycerol was used for all electrical transport measurements, e.g. Fig. 1 of the main manuscript. A second measurement of the magnetic susceptibility was done with glycerol as a pressure medium as presented in Fig. S2.

The comparison of $T_c(P)$ from these three measurements shows very good agreement up to $P = 5.5$ GPa (cf. Fig. S1(a)). This corresponds to the hydrostatic limit of glycerol which undergoes a glass transition around this pressure at 300 K [1]. Above 5.5 GPa, $T_c(P)$ is reduced for the samples in glycerol pressure medium. We attribute this reduction of T_c to a uniaxial compression along the crystallographic c axis of the sample as samples were mounted with the crystallographic c -direction perpendicular to the anvil cutlets [2, 3]. Pressure has been applied at room temperature and the pressure cells have been warmed to 300(1) K after application of pressure. We conclude that glycerol provides high-quality hydrostatic conditions for 2H-NbSe₂ up to 5.5 GPa.

Our measurements of $T_c(P)$ differ significantly from previous studies extending to beyond the critical pressure of the CDW as highlighted in Fig. S1(b) [4, 5]. In order to identify the cause for these differences, we have studied the relevance of the pressure medium and sample preparation. As discussed above, we find a reduced T_c in non-hydrostatic

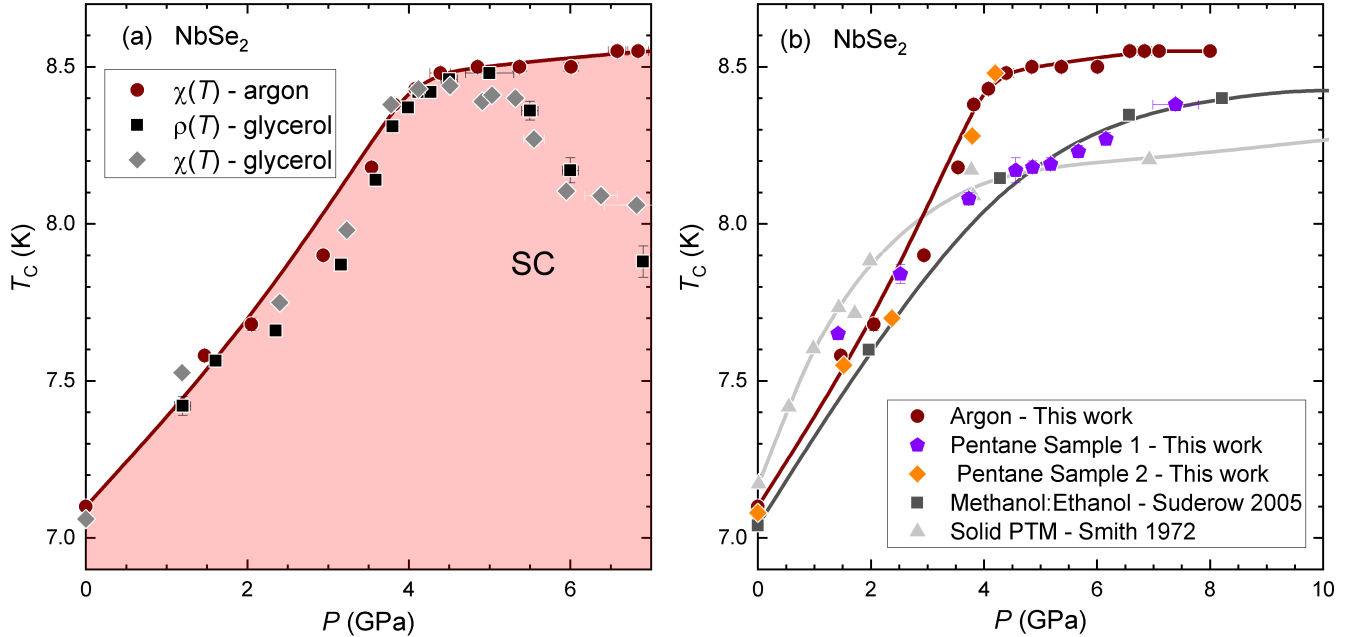


FIG. S1. Superconductivity in 2H-NbSe₂. (a) Comparison of measurements using argon and glycerol as pressure media. (b) Comparison of our measurements with previous studies beyond the CDW critical pressure [4, 5].

conditions for glycerol above 5.5 GPa. Thus, we conclude that the reduced T_c observed by Smith et al [4] is due to the usage of a solid pressure medium.

Suderow et al. used methanol:ethanol which provides good hydrostatic conditions up to 10 GPa [6]. Yet, T_c is reduced and a much smoother rise of $T_c(P)$ is observed by Suderow et al.. We could reproduce the behaviour seen by Suderow et al. in one measurement using pentane:isopentane as a pressure medium (sample 1 in Fig. S1(b)). Pentane:isopentane is very similar to methanol:ethanol and provides good hydrostatic conditions to 10 GPa [6]. A second sample measured in pentane:isopentane, however, followed the $T_c(P)$ of our argon measurements (sample 2 in Fig. S2(b)). Thus, we conclude that the differences in $T_c(P)$ are not due to the pressure medium used as long as it provides good hydrostatic conditions.

We could identify a difference in the sharpness of the superconducting transition in $\chi(T)$ to correlate with the behaviour of $T_c(P)$: For all samples showing the clear kink in $T_c(P)$ (as observed with argon PTM), transitions in $\chi(T)$ are very sharp (see Fig. 3 of the main text and Fig. S2(a) and (c)). For samples with a reduced T_c and a smooth rise in $T_c(P)$, transitions in $\chi(T)$ are much broader (Fig. S2(b)). We note that the broad transitions in glycerol above the solidification pressure (Fig. S2(a) for $P \gtrsim 5.5$ GPa) are attributed to the uniaxial component of the pressure as discussed above. With two samples measured in pentane:isopentane following different behaviour in $T_c(P)$ and in $\chi(T)$ we identify the differences to arise from sample preparation. Indeed, sample 2 and our sample in argon have been screened for sharp transitions at ambient pressure before the study.

With best hydrostatic conditions and sharp transitions in $\chi(T)$ correlated to a sharp kink in $T_c(P)$ at the critical pressure of the CDW we conclude that the behaviour observed with argon as a pressure medium reveals the intrinsic behaviour of 2H-NbSe₂ under pressure.

HIGH-PRESSURE HALL EFFECT MEASUREMENTS

The phase boundary $T_{CDW}(P)$ has been extracted from both dR_H/dT and $R_H(P)$ presented for measurements in $\mu_0 H = 10$ T in the main manuscript. An important observation is the abrupt drop of T_{CDW} at 4.4 GPa. This is best seen in $R_H(P)$ in the inset of Fig. 1 of the main text.

In Fig. 1 of the main manuscript we extract the CDW temperature from the position of the peak in dR_H/dT . No peak is present for pressures $P > 4.4$ GPa in the accessible temperature range. In Fig. S3 we show that the amplitude of the peak diminishes at 4.3(1) GPa. This suggests that the CDW transition is absent above 4.4 GPa.

Further evidence for the absence of the CDW arises from the pressure dependence $R_H(P)$. In Fig. S4 we show $R_H(P)$ for further temperatures. At $T \leq 10$ K, a single kink is observed in $R_H(P)$. At 15 K and 20 K, two kinks are visible in $R_H(P)$. The kink at 3.8(1) GPa and 3.5(2) GPa, respectively from the steepest slope to a very much reduced slope matches with the phase boundary $P_{CDW}(T)$. At $T \leq 10$ K the steepest part of $R_H(P)$ has a similar steep slope compared to 15 K and 20 K. Thus, we identify the low-pressure kink at 15 K and 20 K and the single kink at $T \leq 10$ K with the boundary of the CDW phase.

At 15 K and 20 K, a second kink at 4.4 GPa towards constant $R_H(P)$ happens at the same pressure like the single kink at 5 K and 10 K. The origin of this second kink remains elusive and we can only speculate that it is related to fluctuations of the CDW order for pressures below 4.4 GPa. In fact, strong fluctuations have been inferred from ARPES experiments [7] and mode-mode-coupling calculations [8].

In Fig. S5 we show $R_H(P)$ extracted at $\mu_0 H = 2$ T, i.e. a field just above the critical field of the superconducting state. We find the same behaviour: A kink in $R_H(P)$ at 4.4 GPa which does not shift between 5 K and 10 K, i.e. a very steep phase boundary of $T_{CDW}(P)$ at 4.4 GPa. Thus, we observe that the drop in $T_{CDW}(P)$ is not due to the effect of a finite magnetic field on the CDW transition. This argument is extended to lower fields by the observation of linear $H_{c2}(T)$ at 4.5 GPa presented in Fig. 4(a) with no indications of a change in slope expected for a transition from the CDW state to the pure superconducting state (cf. Fig. 4(b) of the main text).

HIGH-PRESSURE RESISTIVITY MEASUREMENTS

Fig. S6 shows a zero-pressure resistivity trace and its temperature derivative for a sample from the same batch like the high-pressure measurements. The CDW transition is observed at 33.4 K.

Fig. S7 shows the signature of the CDW in the electrical resistivity in our high-pressure measurements. We trace $T_{CDW}(P)$ as the minimum in $d\rho/dT$ as shown in the inset of Fig. S7.

The upper critical field $H_{c2}(T)$ has been extracted from temperature sweeps measuring T_c at a fixed field. At each field T_c was determined as the temperature where the resistivity reaches 10% of the normal state value (see Fig. S8).

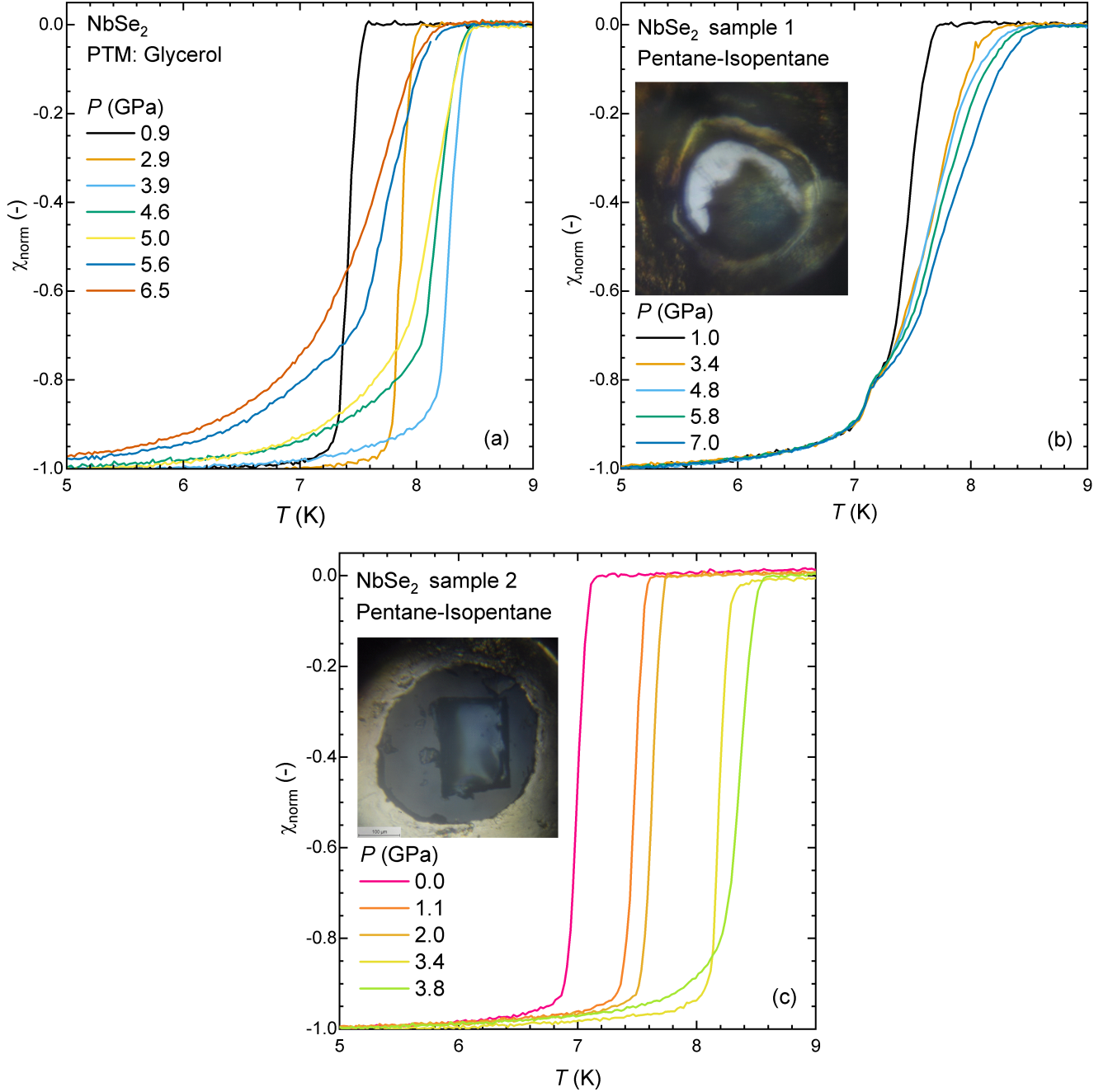


FIG. S2. Superconducting transition of 2H-NbSe₂ in a pressure cell using glycerol as the pressure transmitting medium (a). After subtraction of the background as described in the Methods section of the main manuscript, χ has been normalised $\chi_{\text{norm}}(T) = (\chi(T) - \chi(9\text{K})) / (\chi(9\text{K}) - \chi(4\text{K}))$. Measurements were done during heating up in $\mu_0 H = 0.5\text{ mT}$ after zero-field cooling. Pictures in (b) and (c) show the sample inside the pressure cell at high pressures.

We use the Ginzburg-Landau equation

$$\left. \frac{d\mu_0 H_{c2}}{dT} \right|_{T_c} = - \frac{2.83\pi^2 k_B^2 T_c}{eh v_F^2} \quad (\text{S1})$$

to extract the Fermi velocity v_F from the slope of the critical field. Our measurements show a linear slope over a similar large temperature range as previous studies [9].

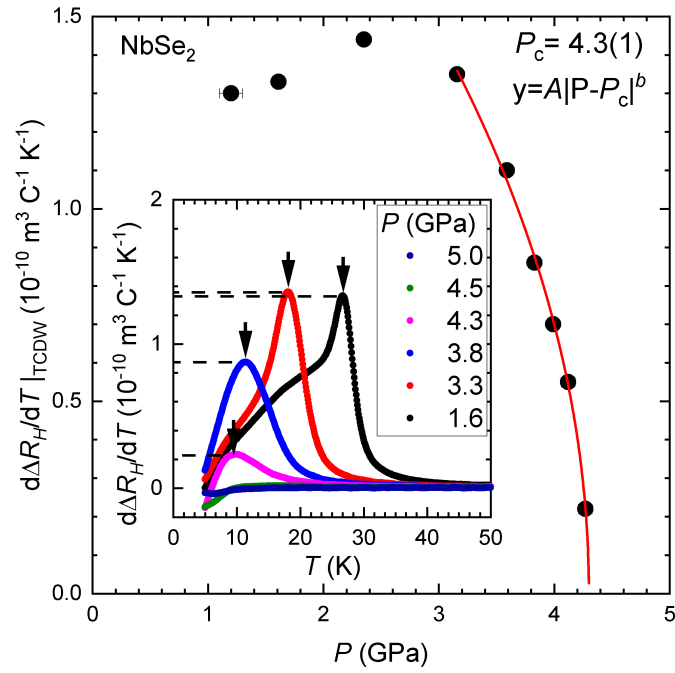


FIG. S3. Amplitude of the peak in dR_H/dT . Main panel shows the height of the peak as a function of pressure with an empirical power-law fit to the data above 3 GPa giving a critical pressure $P_c = 4.3(1)$ GPa. The inset illustrates the height of the peak for different pressures (horizontal dashed lines).

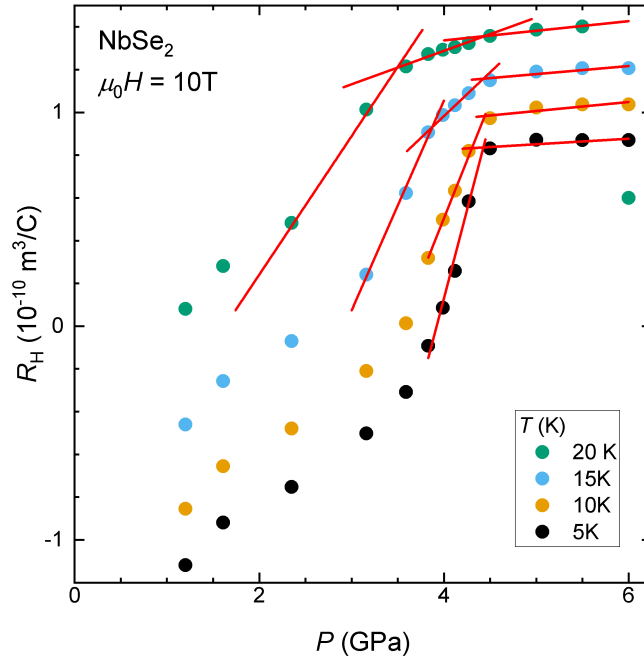


FIG. S4. Pressure dependent Hall coefficient $R_H(P)$ at selected temperatures. Straight lines highlight linear fits to the data.

BACKGROUND SUBTRACTION IN MAGNETIC MEASUREMENTS

A pressure cell mirror symmetric about the sample position was used. Thus, the MPMS software is able to reliably fit a dipole function with the amplitude giving the total magnetic moment of the sample and pressure cell. We remove

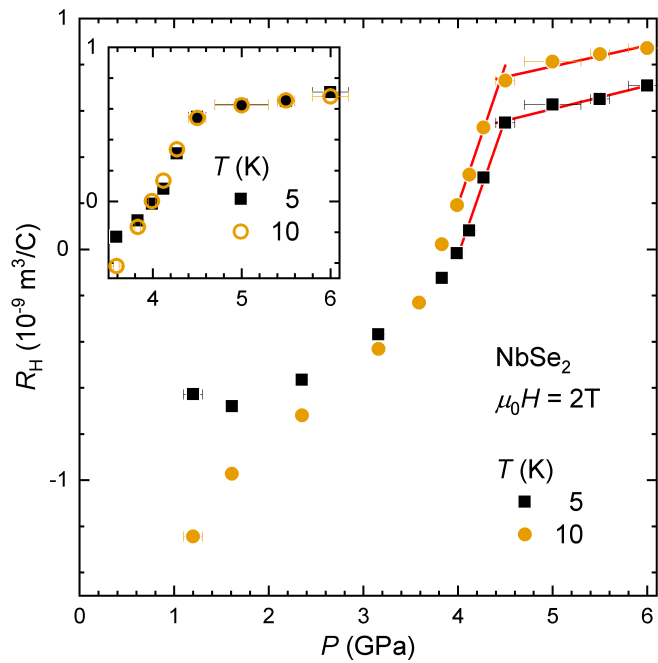


FIG. S5. Pressure dependence of the Hall coefficient at $\mu_0 H = 2$ T for $T = 5$ K and $T = 10$ K. Straight lines show linear fits. The $T=10$ K data has been offset in the inset to match the high-pressure value of the $T=5$ K data.

the background contribution arising from the pressure cell by subtracting a Curie-Weiss type contribution fitted to the field-cooled measurement as illustrated in Fig. S9.

The demagnetisation factor, D , of the sample was calculated using the rectangular prism approximation [10]. The magnetic susceptibility, χ , is calculated from the sample magnetic moment m_s , sample volume V_s , and the applied static magnetic field H as

$$\chi = \frac{m_s}{V_s H} (1 - D). \quad (\text{S2})$$

Small variations in χ at low temperatures are associated with uncertainty of the sample position relative to the SQUID pick-up coils.

CALCULATION OF THE CHARGE-DENSITY-WAVE TRANSITION TEMPERATURE

We employed diagrammatic expansions based on the Random Phase Approximation (RPA), assuming the CDW to develop from a structured electron-phonon coupling dependent on both the ingoing and outgoing electron momenta and the orbital content of the bands. This model, which has as its only free parameter the overall magnitude of the electron-phonon coupling (fixed by $T_{\text{CDW}}(P = 0)$), has previously been shown to agree well with the full range of experimental observations on the charge ordered state in 2H-NbSe₂.

The Random Phase Approximation provides the following expression for the softening of the bare (high-temperature) phonon mode $\Omega_0(q)$ as a function of momentum transfer \mathbf{q} as the temperature decreases towards the CDW phase transition at T_{CDW} :

$$\Omega(q, T)^2 = \Omega_0(q)(\Omega_0(q) - D_2(q, T))$$

where $D_2(q, T)$ is the generalized susceptibility to CDW formation [8, 11, 12]. $D_2(q, T)$ is the Lindhard function convolved with the square of the electron-phonon coupling. As temperature decreases $D_2(q, T)$ increases until, at T_{CDW} and wavevector $Q_{\text{CDW}} \approx 0.986 \cdot \frac{2}{3} \Gamma M$, $D_2(Q_{\text{CDW}}, T_{\text{CDW}}) = \Omega_0(Q_{\text{CDW}})$, and Ω softens to zero. A CDW with wavevector Q_{CDW} results. The one free parameter in the model, the magnitude of the electron-phonon coupling, is set to give the measured value of $T_{\text{CDW}} = 33.4$ K at $P = 0$.

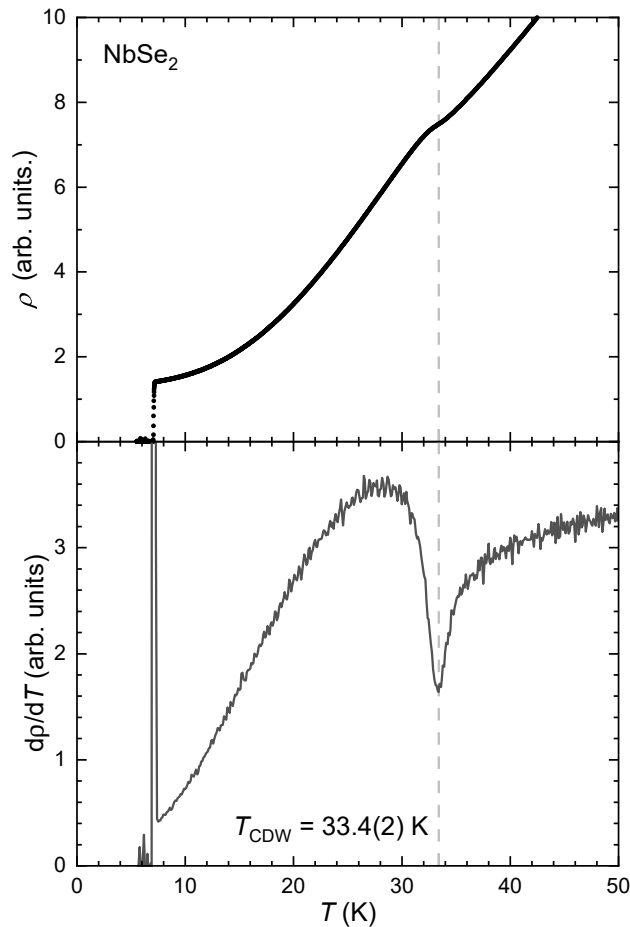


FIG. S6. Zero-pressure resistivity measurements on a sample of 2H-NbSe₂ from the same batch as used for the high-pressure resistivity measurements.

Generally, the effect of increased pressure is to increase the frequency of phonons. Thus, we model high pressures as an increase of Ω_0 , the frequency of the longitudinal acoustic mode from which the CDW develops in 2H-NbSe₂. We find that the momentum transfer q at which $D_2(q, T)$ peaks is largely independent of temperature down to $T = 0$ in agreement with temperature and pressure-dependent X-ray diffraction results [13]. Thus, we can obtain the pressure dependence of T_{CDW} from $D_2(Q_{\text{CDW}}, T = 0)$ using the ambient-pressure Q_{CDW} .

As a consequence of the increase of $\Omega_0(Q_{\text{CDW}})$ at higher pressures, a larger $D_2(Q_{\text{CDW}}, T)$ is required to reach $\Omega = 0$ necessary to achieve the CDW transition. As D_2 increases with decreasing temperature, this corresponds to a decrease in T_{CDW} with pressure. In our model calculations, we analyse the isothermal behaviour: For a fixed $D_2(Q_{\text{CDW}}, T)$, i.e. for a fixed temperature, we find the pressure $P_{\text{CDW}}(T)$ at which $\Omega(q, T)^2 = 0$ corresponding to the boundary of the CDW phase. The value of $D_2(Q_{\text{CDW}}, T = 0)$ sets the maximum bare phonon energy (and therefore pressure) from which a CDW can develop. From this we extract a pressure scaling factor to fit the experimentally observed phase boundary. This scaling corresponds to a rate of stiffening of the bare phonon mode. Finally, by inverting the relation we obtain $T_{\text{CDW}}(P)$, the phase boundary plotted in Fig. 2 of the main manuscript.

CALCULATION OF THE SUPERCONDUCTIVITY TRANSITION TEMPERATURE

Our calculation of T_c as a function of pressure is based on the change of the density of states (DoS) at the Fermi level, $g_{E_F}(\Delta_{\text{CDW}})$, as a function of the CDW gap magnitude Δ_{CDW} .

The total DoS $g_{E_F}(\Delta_{\text{CDW}})$ is calculated from the contributions of the two Nb $d_{3z^2-r^2}$ orbitals $g_{E_F}^{\text{Nb}}(\Delta_{\text{CDW}})$, captured by our model of the Fermi surface developed in Refs. [8, 11, 12]. We add a contribution $g_{E_F}^{\text{Se}}(\Delta_{\text{CDW}})$ from the selenium

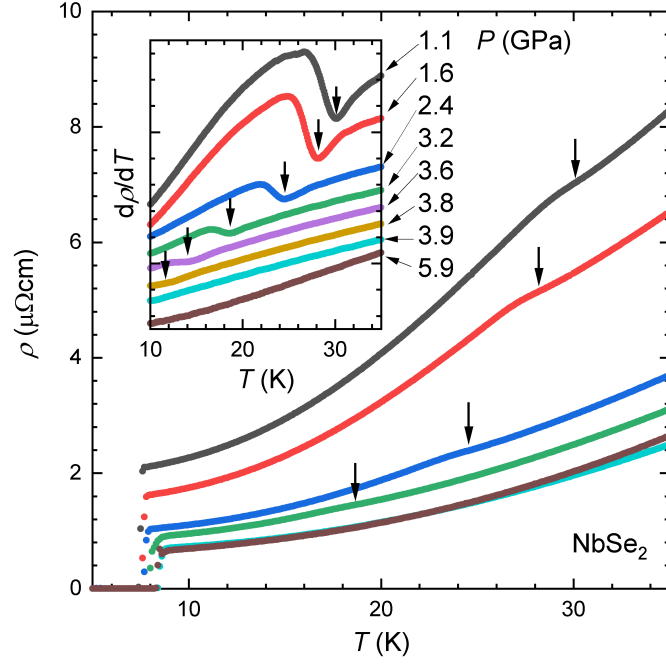


FIG. S7. Electrical resistivity at selected pressures. Inset shows the derivative $d\rho/dT$. Data in the inset have been offset for clarity. Arrows indicated the minimum in $d\rho/dT$ on both panels.

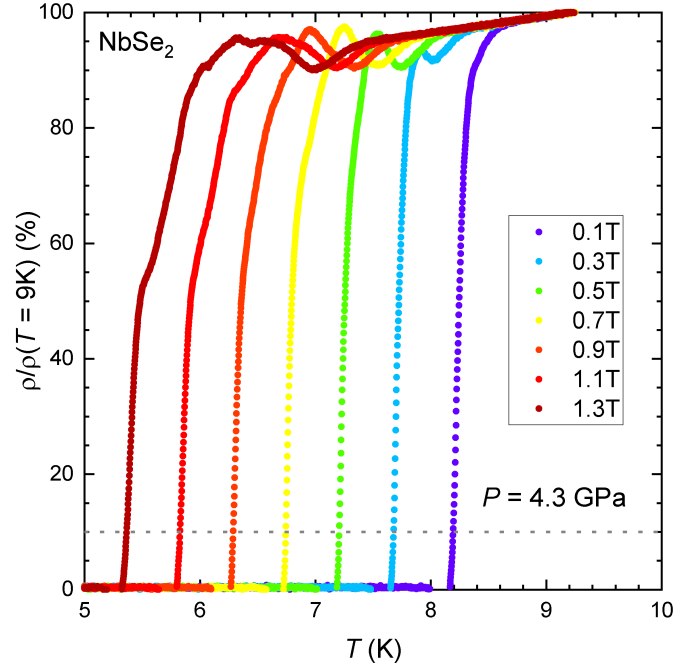


FIG. S8. Resistivity of 2H-NbSe₂ normalised to the normal state resistivity at $T = 9\text{K}$. Dotted line indicates 10% which was used to determine the critical field $H_{c2}(T)$ presented in Fig. 4 of the main text.

band such that the total matches the Sommerfeld coefficient [14].

The DoS of the Nb orbitals was calculated as the sum over the Brillouin zone of the spectral function $A(E, \mathbf{k})$:

$$g^{\text{Nb}} = \frac{1}{N} \sum_{\mathbf{k} \in \text{BZ}} A(E, \mathbf{k}) = -\frac{1}{\pi N} \Im \sum_{\mathbf{k} \in \text{BZ}} G(E, \mathbf{k})$$

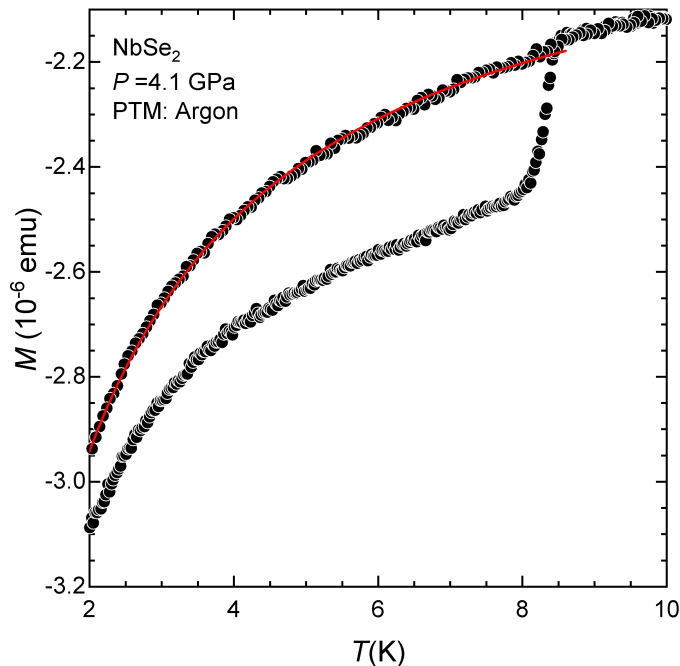


FIG. S9. Magnetic moment of the pressure cell with 2H-NbSe₂ sample on warming after zero-field cooling and on field cooling in $\mu_0 H = 0.5$ mT. The red line shows the Curie-type fit of the background.

where $G(E, \mathbf{k})$ is the retarded electronic Green's function at energy E and wavevector \mathbf{k} . We calculated the Green's function, including the CDW gap, using the Nambu-Gor'kov method [8]. For the wavevector dependence of the CDW gap we solved for the gap self-consistently at six high-symmetry points across the Brillouin zone, and used the results to create a six-parameter tight-binding fit. This calculation was previously shown to give a good match to scanning tunneling spectroscopy measurements of $g(E)$ over a range of energies around E_F [15]. Fig. S10 shows this result. Note that the CDW gap is centred 16 meV above E_F ; nevertheless, it is g_{E_F} which is relevant for the formation of superconductivity.

We simulate the pressure dependence of T_c assuming that Δ_{CDW} varies from the zero-pressure value $\Delta_0 = 12$ meV down to zero. We obtain the DoS of the Nb orbitals $g_{E_F}^{\text{Nb}}(\Delta_{\text{CDW}})$ as shown in Fig. S11. We assume a BCS temperature dependence of $\Delta_{\text{CDW}}(T)$ at a given pressure to obtain $g_{E_F}^{\text{Nb}}(\Delta_{\text{CDW}})$ at the superconducting transition temperature self consistently.

We relate the CDW gap to pressure by scaling to the fitted $T_{\text{CDW}}(P)$ in Fig. 2(a):

$$P = P_{\text{CDW}}(T = 0) \left[1 - \left(\frac{\Delta_{\text{CDW}}}{\Delta_0} \right)^{1/n} \right] \quad (\text{S3})$$

where n and $P_{\text{CDW}}(T = 0)$ are the exponent and critical pressure from the fit to the phase boundary (solid line in Fig. 2).

In order for the total density of states g_{E_F} to be consistent with the Sommerfeld coefficient, we add a constant value of 0.0013 meV^{-1} which is associated with the DoS from the Se-orbitals.

We use the BCS expression to calculate the transition temperature of the superconducting state

$$T_c = 1.14\Theta \exp\left(-\frac{1}{g_{E_F}V}\right)$$

where the coupling constant $V = 0.035$ was obtained to fit the zero-pressure T_c using the zero-pressure g_{E_F} (which is consistent with the experimentally determined DoS from the Sommerfeld coefficient).

* Sven.Friedemann@bristol.ac.uk

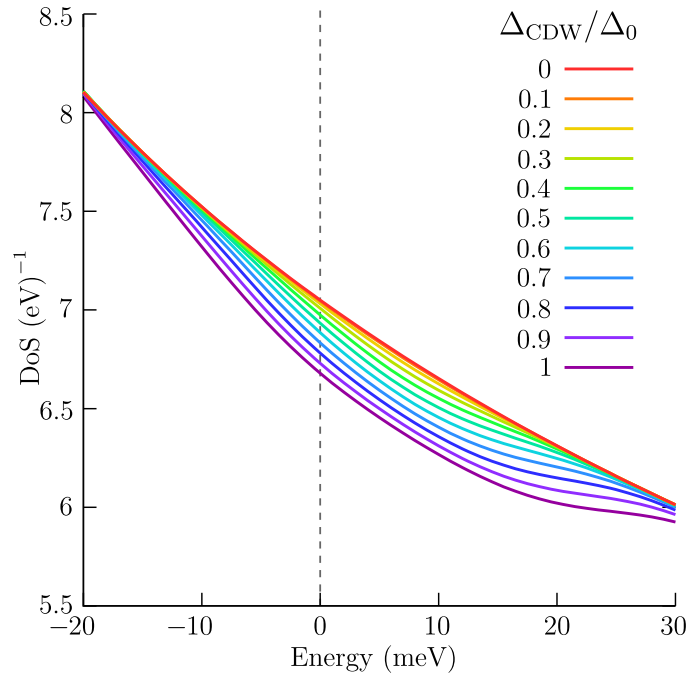


FIG. S10. Density of states $g^{\text{Nb}}(E)$ of the Nb orbitals as a function of energy for different values of the gap, normalised to the gap value at zero pressure. The energy is given relative to E_F .

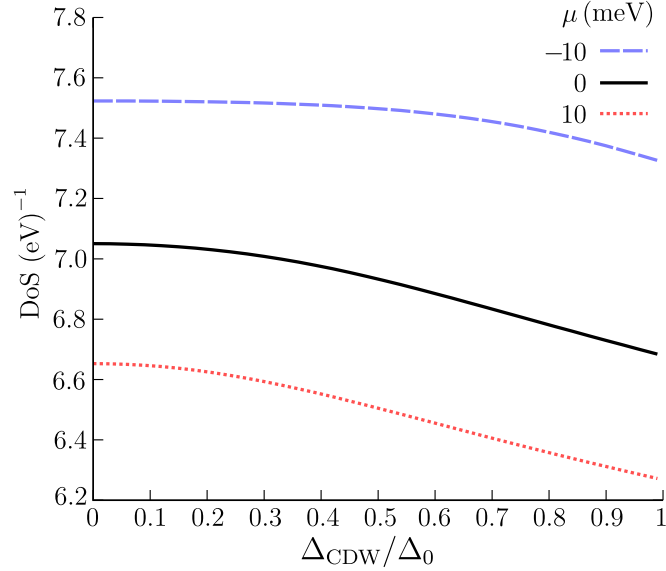


FIG. S11. Density of states $g_{E_F}(\Delta_{\text{CDW}})$ at the Fermi level as a function of the CDW gap size Δ_{CDW} .

- [1] A. Drozd-Rzoska, S. J. Rzoska, M. Paluch, A. R. Imre, and C. M. Roland, On the glass temperature under extreme pressures, *The Journal of Chemical Physics* **126**, 164504 (2007).
- [2] A. Wieteska, B. Foutty, Z. Guguchia, F. Flicker, B. Mazel, L. Fu, S. Jia, C. Marianetti, J. van Wezel, and A. Pashupathy, Uniaxial Strain Tuning of Superconductivity in $2H\text{-NbSe}_2$, arXiv:1903.05253 [cond-mat.supr-con] (2019), <http://arxiv.org/abs/1903.05253v1>.
- [3] T. Sambongi, Effect of uniaxial stress on the superconducting transition temperature of NbSe_2 , *Journal of Low Temperature Physics* **18**, 139 (1975).
- [4] T. F. Smith, L. E. DeLong, A. R. Moodenbough, T. H. Geballe, and R. E. Schwall, Superconductivity of NbSe_2 to 140 kbar, *Journal of Physics C: Solid State Physics* **5**, L230 (1972).
- [5] H. Suderow, V. Tissen, J. Brison, J. Martínez, and S. Vieira, Pressure Induced Effects on the Fermi Surface of Supercon-

- ducting 2H-NbSe₂, *Phys. Rev. Lett.* **95**, 117006 (2005).
- [6] N. Tateiwa and Y. Haga, Evaluations of pressure-transmitting media for cryogenic experiments with diamond anvil cell., *Rev. Sci. Instrum.* **80**, 123901 (2009).
- [7] S. V. Borisenko, A. A. Kordyuk, V. B. Zabolotnyy, D. S. Inosov, D. Evtushinsky, B. Büchner, A. N. Yaresko, A. Varykhalov, R. Follath, W. Eberhardt, L. Patthey, H. Berger, and B. Buchner, Two Energy Gaps and Fermi-Surface "Arcs" in NbSe₂, *Phys. Rev. Lett.* **102**, 166402 (2009).
- [8] F. Flicker and J. van Wezel, Charge order in NbSe₂, *Phys. Rev. B* **94**, 235135 (2016).
- [9] B. J. Dalrymple and D. E. Prober, Upper critical fields of the superconducting layered compounds Nb_{1-x}Ta_xSe₂, *Journal of Low Temperature Physics* **56**, 545 (1984).
- [10] A. Aharoni, Demagnetizing factors for rectangular ferromagnetic prisms, *Journal of Applied Physics* **83**, 3432 (1998), <https://doi.org/10.1063/1.367113>.
- [11] F. Flicker and J. van Wezel, Charge order from orbital-dependent coupling evidenced by NbSe₂, *Nature Communications* **6**, 7034 (2015).
- [12] F. Flicker and J. van Wezel, Charge ordering geometries in uniaxially strained NbSe₂, *Phys. Rev. B* **92**, 201103 (2015).
- [13] Y. Feng, J. van Wezel, J. Wang, F. Flicker, D. M. Silevitch, P. B. Littlewood, and T. F. Rosenbaum, Itinerant density wave instabilities at classical and quantum critical points, *Nature Physics* **11**, 865 (2015).
- [14] C. L. Huang, J.-Y. Lin, Y. T. Chang, C. P. Sun, H. Y. Shen, C. C. Chou, H. Berger, T. K. Lee, and H. D. Yang, Experimental evidence for a two-gap structure of superconducting NbSe₂: A specific-heat study in external magnetic fields, *Phys. Rev. B* **76**, 212504 (2007).
- [15] A. Soumyanarayanan, M. M. Yee, Y. He, J. van Wezel, D. J. Rahn, K. Rossnagel, E. W. Hudson, M. R. Norman, and J. E. Hoffman, Quantum phase transition from triangular to stripe charge order in NbSe₂., *Proc. Natl. Acad. Sci. U. S. A.* **110**, 1623 (2013).